HHS Public Access

Author manuscript

J Neurosci Methods. Author manuscript; available in PMC 2022 August 01.

Published in final edited form as:

J Neurosci Methods. 2021 August 01; 360: 109270. doi:10.1016/j.jneumeth.2021.109270.

Development of a protocol to assess within-subject, regional white matter hyperintensity changes in aging and dementia

Ahmed A. Bahrani[a,b,j], **Charles D. Smith**[a,c,d], **Justin M. Barber**[a], **Omar M. Al-Janabi**[a], **David K. Powell**[c], **Anders H. Andersen**[c], **Brandon D. Ramey**[a], **Erin L. Abner**[a,e,f], **Larry B. Goldstein**[d], **Zachary Winder**[a,g], **Brian T. Gold**[a,h], **Linda Van Eldik**[a], **Donna M. Wilcock**[a,h], **Gregory A. Jicha**[a,d,i]

[a]Sanders-Brown Center on Aging, University of Kentucky, Lexington, KY 40506, USA

[b]Department of Biomedical Engineering, University of Kentucky, Lexington, KY 40506, USA

[c]Magnetic Resonance Imaging and Spectroscopy Center (MRISC), University of Kentucky, Lexington, KY 40506, USA

[d]Departments of Neurology, University of Kentucky, Lexington, KY 40506, USA

[e]Department of Epidemiology, University of Kentucky, Lexington, KY 40506, USA

[f]Department of Biostatistics, University of Kentucky, Lexington, KY 40506, USA

[g]Department of Physiology, University of Kentucky, Lexington, KY 40506, USA

[h]Department of Neuroscience, College of Medicine, University of Kentucky, Lexington, KY 40536, USA

[I] Departments of Behavioral Science, University of Kentucky, Lexington, KY 40536, USA

[j]Biomedical Engineering Department, Al-Khwarizmi College of Engineering, University of Baghdad, Baghdad, Iraq

Corresponding author: Gregory A. Jicha, MD-PhD, Sanders-Brown Center on Aging, 800 South Limestone St, Lexington, KY 40536-0230, gregory.jicha@uky.edu.

Credit Author Statement

Methodology: Ahmed A. Bahrani, Charles D. Smith
Data curation: Ahmed A. Bahrani, Justin M. Barber, Erin L. Abner, Zachary Winder
Software: Ahmed A. Bahrani
Formal analysis: Ahmed A. Bahrani, Brandon Ramey, Omar M. Al-Janabi
Validation: Ahmed A. Bahrani, Omar M. Al-Janabi
Visualization: Ahmed A. Bahrani, Gregory A. Jicha, Charles D. Smith,
Investigation: Ahmed A. Bahrani, Charles D. Smith, Gregory A. Jicha
Supervision: Charles D. Smith, Gregory A. Jicha, David K. Powell, Anders H. Andersen, Ahmed A. Bahrani
Project administration: Gregory A. Jicha
Funding acquisition: Gregory A. Jicha, Donna M. Wilcock
Resources: Gregory A. Jicha
Writing - Original Draft: Ahmed A. Bahrani
Writing – review & editing: Gregory A. Jicha, Charles D. Smith, David K. Powell, Anders H. Andersen, Erin L. Abner, Brian T. Gold, Justin M. Barber, Larry B. Goldstein, Linda Van Eldik, Donna M. Wilcock

Disclosures: The author and the co-authors have no conflict of interest related to the present study.

Abstract

Background: White matter hyperintensities (WMH), associated with both dementia risk and progression, can individually progress, remain stable, or even regress influencing cognitive decline related to specific cerebrovascular-risks. This study details the development and validation of a registration protocol to assess regional, within-subject, longitudinal WMH changes (ΔWMH) that is currently lacking in the field.

New Method: 3D-FLAIR images (baseline and one-year-visit) were used for protocol development and validation. The method was validated by assessing the correlation between forward and reverse longitudinal registration, and between summated regional progression-regression volumes and Global ΔWMH. The clinical relevance of growth-regression ΔWMH were explored in relation to an executive function test.

Results: MRI scans for 79 participants (73.5±8.8 years) were used in this study. Global ΔWMH vs. summated regional progression-regression volumes were highly associated (r^2 =0.90; p-value<0.001). Bi-directional registration validated the registration method (r^2 =0.999; p-value<0.001). Growth and regression, but not overall ΔWMH, were associated with one-year declines in performance on Trial-Making-Test-B.

Comparison with Existing Method(s): This method presents a unique registration protocol for maximum tissue alignment, demonstrating three distinct patterns of longitudinal within-subject ΔWMH (stable, growth and regression).

Conclusions: These data detail the development and validation of a registration protocol for use in assessing within-subject, voxel-level alterations in WMH volume. The methods developed for registration and intensity correction of longitudinal within-subject FLAIR images allow regional and within-lesion characterization of longitudinal ΔWMH. Assessing the impact of associated cerebrovascular-risks and longitudinal clinical changes in relation to dynamic regional ΔWMH is needed in future studies.

GRAPHICAL ABSTRACT

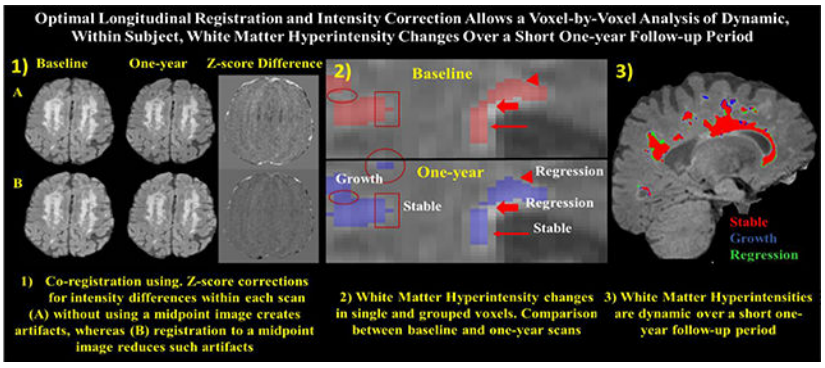

Tracking dynamic changes in white matter hyperintensities (WMH) is critical for the assessment of longitudinal degenerative and vascular disease related injury. WMHs have been shown to progress, remain stable, or even regress over time. The present study sought to develop and validate a registration protocol that will allow the assessment of regional, within-subject, longitudinal WMH changes over periods as short as one-year, necessary for use in future clinical

trials of disease modifying therapies that hope to limit, stabilize, or even reverse deleterious WMH injury.

Keywords

Longitudinal; White matter hyperintensity; Aging; Dementia; Small vessel ischemic disease; Cerebrovascular disease

1. Introduction

White matter hyperintensities (WMH), visualized on magnetic resonance imaging (MRI) T2-weighted fluid-attenuated inversion recovery (FLAIR) images, are a critical biomarker in the study of cerebrovascular small vessel ischemic disease (SVID) (Wang et al. 2020), an important contributor to cognitive decline and development of dementia (Kandel et al. 2016, Habes et al. 2016, Prabhakaran 2019, Brugulat-Serrat et al. 2020, Zhao et al. 2019). WMH volumetric assessment has contributed to the understanding of SVID and its impact on cognitive status in both normal aging and dementia (d'Arbeloff et al. 2019), demonstrating strong associations with both memory and executive function (Brickman, Muraskin, and Zimmerman 2009, Iorio et al. 2013, Rost et al. 2014, Tsai, Peng, et al. 2014, Valdes Hernandez et al. 2017). Although WMHs occur in many disease states, in the aging population they are most frequently associated with SVID and cerebrovascular disease (CVD) risk factors including poorly controlled hypertension, hyperlipidemia, and diabetes (Kalaria and Erkinjuntti 2006, Murray et al. 2012). Few studies, however, have explored the development of longitudinal WMH volumetric quantification techniques that can track longitudinal, within-person, regional WMH changes (Al-Janabi et al. 2019, Ramirez et al. 2016).

Total WMH volumes are dynamic over time and frequently progress (Ramirez et al. 2016, Silbert et al. 2008), but in a substantial proportion of persons WMH may be stable or even regress over time (van Leijsen et al. 2019, van Leijsen et al. 2017, Al-Janabi et al. 2019). We hypothesize that the dynamic nature of WMH may not be evident when analyses are limited to assessment of total WMH volumes, as different regions and or discrete WMH lesions may differentially exhibit growth (Dickie et al. 2016), stability (Lauer et al. 2021) and or regression (van Leijsen et al. 2019, van Leijsen et al. 2017, Al-Janabi et al. 2019). Thus, in many individuals, the total WMH volume change may represent a cancellation of WMH growth and regression that co-occur, albeit in different neuroanatomic and or lesional distributions. We further hypothesize that although progression of WMH likely represents tissue damage associated with poorly controlled CVD risks, stability of WMH lesions may suggest adequate control of CVD risks, and regression of WMH may represent intrinsic healing or reparative processes, such as the induction of de novo angiogenesis (Greenberg 2014, He et al. 2017, Raman et al. 2018, Al-Janabi et al. 2019). It is likely that even a single WMH lesion could progress in one neuroanatomic direction and simultaneously regress in another, dependent on the interplay between causative and reparative mechanisms within the local neuroanatomic and neurovascular milieu. Understanding such changes longitudinally in relation to specific neuroanatomic distributions of WMH growth, stability, and regression

has important implications for the understanding of underlying biological mechanisms of WMH change, associations with CVD risk factors, and longitudinal cognitive outcomes.

Developing protocols that allow the quantification of progression, stability, or regression of discrete and regional WMH lesions may help to clarify the relative contributions of risks for WMH progression (e.g., uncontrolled CVD risks) versus mechanisms of healing or repair associated with WMH regression (e.g., induction of angiogenesis (Greenberg 2014, He et al. 2017, Raman et al. 2018), reduction in focal WMH inflammation (Wardlaw et al. 2017, Wardlaw, Valdes Hernandez, and Munoz-Maniega 2015), etc.) that may occur simultaneously. Such techniques could support therapeutic clinical trials targeting CVD risk reduction (reduced progression) or strategies designed to promote WMH healing (enhanced regression). This manuscript details the development and validation of one such longitudinal, within-subject, regional, white matter hyperintensity volumetric protocol.

2. Methods

2.1. Participants

Research volunteers were drawn from the University of Kentucky Sanders-Brown Center on Aging cohort. Details of the recruitment criteria and annual longitudinal examination have been published previously (Schmitt et al. 2012). Participants were included in the current study if they had both a baseline and one year follow up MRI scan that included identical T1 MPRAGE and 3D FLAIR acquisition sequences, irrespective of clinical diagnoses (N = 83). Identical MRI sequences were acquired for each participant on the same scanner at both baseline and one-year follow-up. Four participants were excluded from the analysis on the basis of extreme motion artifact or distortion of normal anatomy required for accurate volumetric processing (Fig. 1).

The study procedures were approved by the University of Kentucky Institutional Review Board (IRB), and written consents were obtained from all participants (or a legally authorized representative for participants without the capacity to provide informed consent).

2.2. MRI acquisition

MRI images were obtained using a 3T TIM-Trio MRI scanner (Siemens Healthcare, Erlangen, Germany) at the Magnetic Resonance Imaging and Spectroscopy Center (MRISC) of the University of Kentucky. All participants underwent two MRI sessions using a 32-channel receiver head coil. The T1-weighted MPRAGE image acquisition parameters were TE 2.3 msec, TR 2,530 msec, TI 1,100 msec, flip angle 7°, and isotropic 1×1×1 mm resolution with full brain coverage. The MPRAGE imaging sequence was repeated twice at both baseline and one year follow up visits for each participant, which were averaged to increase the signal-to-noise ratio. The T2-weighted FLAIR image acquisition parameters were TE 388 msec, TR 6,000 msec, TI 2,200 msec, and isotropic 3D resolution of 1×1×1 mm.

2.3. Image Processing

Image processing parameters were determined for each of four main steps: 1) pre-longitudinal registration, 2) longitudinal registration, 3) segmentation, and 4) generation of WMH masks.

2.3.1. Pre-longitudinal registration—Based on previously published WMH volumetric methods (Bahrani et al. 2017), two anatomical T1-weighted images and one FLAIR image were acquired for each time-point for each participant. Intensity bias was corrected using non-parametric, non-uniform intensity normalization (N3-correction) methods (Sled, Zijdenbos, and Evans 1998, Boyes et al. 2008, Ashburner and Friston 2005). For each time-point, the two anatomical T1-weighted images were co-registered and averaged to optimize the signal-to-noise ratio. The averaged T1-weighted image was subsequently registered to the FLAIR image, using a rigid body registration with 6-parameters, for each time point (Fig. 2) and similarly the follow-up visit FLAIR image co-registered to the baseline FLAIR image (Fig. 2, Fig. 3A and B, and Fig. 4A–C).

2.3.2. Longitudinal Registration—The paired (baseline and follow-up) FLAIR images derived from the pre-longitudinal registration step were used to generate a midpoint image and establish a deformation field for each time-point using the SPM12 longitudinal registration tool (http://www.fil.ion.ucl.ac.uk/spm) (Fig. 5) (Ashburner and Ridgway 2012). The midpoint FLAIR image (Fig. 5 and Fig. 3C) and deformation field maps were used to register the two-time-point images (rT1-BL, rrT1-Y1, T2-BL and rT2-Y1) longitudinally to the midpoint image to reach a maximum alignment of the two images (Fig. 3A–E and Fig. 4D–F). The deformation field map is a matrix that carries the information of the position and magnitude of the deflection in the image space. In our case, this deformation map is generated as an outcome of the longitudinal registration. The deformation field map is utilized in our protocol to apply the stored information that is essential for registering the baseline and one-year images to the midpoint image (Ashburner and Ridgway 2012, Beg and Khan 2007, Hadj-Hamou et al. 2016, Hutton et al. 2002).

The longitudinal registered T1-weighed images (LR-T1-BL and LR-T1-Y1) of the two-time points were averaged to create a midpoint of the T1-weighted image (T1-midpoint, Fig. 5). Both T1-weighted and FLAIR midpoint images were used for the subsequent segmentation protocol.

To ensure the registration algorithm did not create excessive voxel deformation in images between time points, the images from baseline and one-year were registered in two directions. The protocol used the baseline image as a reference, and the image from the one-year visit as a target for all steps (pre-longitudinal and longitudinal steps) to generate the midpoint image (Fig. 3C and Fig. 5). To ensure the registration process did not create bias for one image over another, the algorithm was repeated with a subset of cases, reversing the sequence of the images, i.e., one-year visit as a reference and the baseline as a target (n = 8).

2.3.3. Segmentation—Each FLAIR midpoint image was stripped using the FSL-BET FMRIB software library (FSL v5.0.8) Brain Extraction Tool (http://fsl.fmrib.ox.ac.uk/fsl/fslwiki/BET) to generate FLAIR brain tissue image and binary masks. The binary mask

was multiplied by the T1-midpoint image to create the T1-midpoint brain tissue image. The binary mask was also multiplied by the FLAIR longitudinal registered images to get the FLAIR brain images. Intensity bias correction was run again for the stripped images as described above.

SPM12 was used to perform unified segmentation of the T1- and T2-midpoint brain images based on a custom template that has been described previously (Smith et al. 2016, Bahrani et al. 2017). Five separate native space masks were generated from this segmentation step: gray-matter (GM), two white matter (WM), cerebral spinal fluid (CSF) and unclassified tissue.

2.3.4. Generation of Total WMH Growth and Regression Masks/Volumes: The two-segmented WM tissue class images were summed to obtain the total WM mask, which was converted to a binary mask. The resultant WM binary mask was multiplied by the FLAIR images of each time-point to obtain the total WM tissue intensity image (Fig. 3F). The histogram distribution for each WM mask was fitted to a two-component Gaussian mixture model curve to adapt two components of the WM signal intensities, which included normal-appearing WM and WMH. The mean and standard deviation from the Gaussian curve were used to calculate the maximum (mean + 15 SD) and minimum (mean + 3 SD) intensity thresholding values. Stripped FLAIR images for each time-point were then subject to these thresholding parameters to generate the final raw WMH mask. This mask includes some false-positive artifacts related to intensity overlaps between the normal-appearing WM and the WMH. These artifacts were reduced by performing a median filtering on a slice-by-slice basis using a 3×3 2D kernel filter. Manual editing was required to delete artifactual WMH voxels using the original FLAIR images as a guide (Fig. 3G and 3H) based on a standard editing criterial (Bahrani et al. 2019).

2.3.5. Generation of Regional WMH Growth and Regression Masks/Volumes —Regional WMH masks were generated based on simple subtraction between the total WMH masks described above. Specifically, the one-year time point, and baseline time point total WMH masks were subtracted from each other in order to generate the regional growth and regression represent regression (shrinkage) of the WMH volume. An example of a single subject's data showing voxels characterized by growth, regression and stability is presented in Fig. 3I, Fig. 6 and Fig. 7.

A subset of 30 participant scans were analyzed using both the longitudinal regional methods presented in this manuscript and also using standardized cross sectional volumetrics method that we previously published (Bahrani et al. 2019, Bahrani et al. 2017) for each time point independently. The total volume difference between progression and regression (P-R) within each participant was compared to the WMH volume difference (WMH2-WMH1) for each participant.

The protocol was scripted for automated application within a Singularity container (https://singularity.lbl.gov/) to streamline the process. Despite an attempt to fully automate the protocol, the pipeline still requires a manual editing step to be performed on the final

composite WMH mask to remove any false positive voxels before generating the WMH growth and regression masks.

2.4. Exploring the potential clinical utility of WMH growth/regression

Clinically, deficits in processing speed and executive function on neuropsychological testing are a hallmark of SVID (Lamar et al. 2010). Trail Making Test (TMT) A (processing speed) and B (executive function) were used to evaluate the potential clinical utility of the protocol. TMT was administered at the time of the first and second MRIs. Difference scores for TMT-A and TMT-B were computed as difference in completion time (i.e., second scan minus first scan). Both difference scores were roughly normal upon visual inspection and not subject to transformation. Negative values represented improvement.

For the analysis, WMH growth was computed as $progression / ([TIV1 + TIV2] / 2)$ and WMH regression was computed as $regression / ([TIV1 + TIV2] / 2)$. Both were highly right-skewed and subjected to square root transformation for analysis. Total WMH change was computed as $(WMH2 – WMH1) / ([TIV1 + TIV2] / 2)$. Several transformations were attempted, but none improved nonnormality and the raw value was used in analysis.

2.5. Statistical Analysis

SPSS 23.0 was used to calculate Pearson's correlations in the evaluation of co-registration and intensity correction techniques and the relation of the experimental growth/regression protocol to longitudinal WMH volume changes. The R v4.0.0 console (Team 2013, Wickham 2016) was used to perform a preliminary analysis of potential clinical meaningfulness of penumbra data. Backwards selection was applied to two linear regression models, one for each part of the TMT. Age, sex (male or female), education (in years), clinical status at time of first MRI (Association 2013), MCI (Winblad et al. 2004), or cognitively intact, WMH growth, WMH regression, and total WMH change were included as predictors in both initial models. Backwards selection procedures included sequentially removing the predictor with the largest p-value >0.05 until the model fit failed to improve with subsequent backward selection (fit measured using AIC).

3. Results

Paired scans were initially available for 83 participants (baseline and one-year visits). Four subjects were excluded due to either motion artifact or irregular shape of the brain images, demonstrating that the protocol can be successfully applied in over 90% of participants (Fig. 1). Basic demographic and clinical features of the 79 participants are presented in Table 1. A graphical depiction of stable, growth, and regression WMH volumes for all subjects is shown in Fig. 8A. These data demonstrate that while approximately 50% of subjects show no appreciable total WMH volume change over the one-year study period, 19% demonstrate overall regression and 31% exhibit overall growth (right panel). The number of subjects that showed dynamic growth (55%) and regression (31%) in combination (partially cancelling growth and regression volumes out) was much higher than those identified using total WMH volumes above. A sample of three cases shown in Fig. 8B to demonstrate the WMH

difference of the two-time points compared to the longitudinal WMH growth and regression protocol.

3.1. Registration Validation

Forward and reverse longitudinal registrations were significantly associated ($r^2 = 0.999$; p-value < 0.001) supporting our use of a midpoint registration method that was unaffected by variability in discrete scan acquisition.

3.2. Longitudinal registration vs. cross-sectional WMH volume

Total change in WMH volume determined using the longitudinal regional vs. absolute difference in cross sectional WMH volumes were highly related based on a linear regression model ($r^2 = 0.90$, p-value < 0.001).

3.3. Potential clinical utility

TMT from both time points were available for 3 demented, 34 MCI, and 28 cognitively intact participants. Sex was the only predictor retained following backwards selection on the model with TMT-A difference as the dependent variable (being female, $\beta = -8.13$, $p = 0.11$, $\eta^2 = 0.04$). Backwards selection on the model with TMT-B difference as the dependent variable retained education ($\beta = -5.45$, $p = 0.02$, $\eta^2 = 0.06$), WMH growth ($\beta = 429.1$, $p = 0.16$, $\eta^2 = 0.041$), and WMH regression ($\beta = 584.6$, $p = 0.13$, $\eta^2 = 0.034$), but not total WMH change. The model explained about 13.5% of the variation in TMT-B difference scores in this sample, $F(3, 61) = 3.17$, $p = 0.031$, $R^2 = .135$, $_{\text{adjusted}}R^2 = 0.092$.

4. Discussion

These data and the methodology described demonstrate the feasibility of characterizing within-subject, regional changes in WMHs over time. The present investigations focused on validation of a registration pipeline that allows longitudinal regional and within lesion comparisons. A one-year period was used to validate and develop the methods as such a short time frame is ideal for future use in VCID interventional clinical trials. Tracking such WMH changes longitudinally is important for understanding the dynamic nature of WMH and to enable further understanding of vascular imaging abnormalities within and in the immediate vicinity of WMH lesions.

Previous studies assessing total WMH volume change over time have demonstrated that WMH are dynamic, with some participants demonstrating progression (Ramirez et al. 2016), while many others show stability or even regression (Chen et al. 2018, Al-Janabi et al. 2019). Similar results were seen in the present study with total WMH volumes remaining stable in 50% of participants, but demonstrating either total growth or regression in 31% and 19% respectively. It is intriguing that the present results demonstrate ongoing growth and regression in many of the same subjects to a much higher degree, suggesting that WMH lesions may be far more dynamic than envisioned previously. Such findings regarding dynamic WMH change in the elderly are likely the result of fluctuating control of CVD risk factors that lead to progressive vascular injury and or a healing processes that can occur simultaneously. The dynamic nature of WMH is not unprecedented across the spectrum of

neurologic diseases in which WMH are the major imaging finding (Moroni et al. 2018, Williamson et al. 2018, Gunstad et al. 2005). Similar dynamic change in WMH can occur in patients with Multiple Sclerosis (Zhong et al. 2014, Trip and Miller 2005), infectious and inflammatory processes (Sarbu et al. 2016, Pandit 2009), cerebral amyloid angiopathy-related inflammation (Lee et al. 2018, Rigney, Sebire, and Cordato 2015, Makarewicz et al. 2019, Kirshner and Bradshaw 2015), and in amyloid-related imaging abnormalities (ARIA) associated with anti-amyloid therapies for Alzheimer's disease (Gordon et al. 2015, Nasrabady et al. 2018).

Whether longitudinal WMH progression, stability, or regression within all WMHs are uniform in discrete subjects, or whether they are dynamic within subjects and or within discrete lesions has been unclear previously. Despite this lack of understanding, it has been hypothesized that discrete within lesion growth vs. regression may be important in our understanding of the interplay between injurious and reparative vascular processes. The present data demonstrate that such lesion-discrete within subject dynamism is true, with each distinct WMH lesion demonstrating local areas of progression, stabilization, and or regression to varying degrees. Understanding such within lesion areas of focal dynamic WMH change is critical for our understanding of localized neuroanatomic, neurovascular and potentially regional impacts of CVD risk factors in influencing WMH change over time.

Several studies have previously attempted to predict such dynamic changes in WMH and neuroanatomic distribution, popularizing the term "penumbra" to describe such areas of potential change. This concept of a regional area "at-risk" is similar to the concept of a penumbra associated with large-vessel ischemic strokes (Tsai, Yuan, et al. 2014, Wintermark et al. 2006, Saver 2017). Several of these studies focused on specifying the WMH penumbra as the region surrounding observed WMH lesions, within a specific radius agnostic to local neuroanatomy, neurovascular distributions, or actual WMH lesional volume change over time (Baldaranov et al. 2017, Beason-Held et al. 2007, Keihaninejad et al. 2013, Mills and Tamnes 2014). Further advances using such methodology include the development of a probability model to generate a neighborhood WMH injury score that again is agnostic to actual observed changes in discrete WMH lesional volumes (Maillard et al. 2011). Such approaches have identified abnormalities in diffusion tensor imaging fractional anisotropy and arterial spin labeling perfusion, but were unable to detect overt WMH changes within the identified at-risk regions (Maillard et al. 2013, Maillard et al. 2011, Maillard et al. 2012).

Tracking focal within lesion WMH volumetric change is problematic due to a number of factors, most important of which are refining longitudinal co-registration and intensity corrections. The present method of longitudinal registration requires alignment of the ventricular borders. This alignment creates a reference point in relation to WMH changes using the SPM12 toolbox. Ashburner et al. (2013) created the longitudinal registration application with version SPM12 and further referred to the existence of a steeper signal intensity gradient between the two-time-points images after longitudinal registration that was problematic (Ashburner and Ridgway 2012). The explanation for the steeper gradient was not elucidated based on these studies (Ashburner and Ridgway 2012). The present experiments identified a residual linear WMH signal along the ventricular border after the longitudinal registration that contributed to the gradient abnormalities. To overcome

this issue, an extra linear registration step was added to the protocol prior to longitudinal registration to aid in maximal co-registration of images from the two time points. Without such an intermediate step, the z-score difference between the baseline and the one-year images, (see Fig. 4), demonstrates that the longitudinal registration may not always result in an accurate alignment of the FLAIR images. Such misalignment in the longitudinal registration can produce false positive changes in discrete WMHs that largely remain confined to the ventricular boundaries and some gyri. Such findings indicate an inaccurate alignment of the two sets of images rather than true WMH change. The present protocol included an additional rigid body registration prior to the longitudinal registration step that appears to be important for assessing discrete focal lesional WMH changes in all directions.

Even though N3-correction was used in both the longitudinal registration process (Ashburner and Ridgway 2012) and the segmentation process (Ashburner and Friston 2005), we employed this technique again two more times. Once during the pre-longitudinal registration, to increase the quality of the co-registration process of the T1-weighted and FLAIR images to correct the background intensity inhomogeneity resulting from imperfections in the MRI imaging acquisition, and second to remove the residual intensity nonuniformity after the nonbrain tissue extraction of the midpoint images before the segmentation step. The inclusion of the extra intensity bias corrections resulted in an almost zero unclassified tissue volume supporting the importance of such additional N3-correction steps.

Maltbic et al. (2012) found that inherent brain asymmetry influenced the segmentation of the brain structures in the left and right hemisphere (Maltbie et al. 2012). The present data confirm this prior finding (Fig. 1B). The present data also identified significant motion artifacts as barriers to the use of the present protocol as they lead to inaccurate segmentation due to intensity overlaps resulting in either an over- or under-estimated WMH voxels change at the circumferential border of the WMH lesion. Scans with either significant asymmetry or motion artifact should be identified as unsuitable for volume and regional pattern longitudinal WMH analysis prior to investing time and effort and potentially including confounded data in any analyses using this or similar protocols.

We relied on two methods to test the validity of the present protocol. We first validated the registration in two directions by switching the order of the reference image between the baseline and one-year visit. The results of this analysis demonstrated a strong relationship between forward and backward reference comparisons ($r^2 = 0.999$, p-value < 0.001) supporting to the validity of the proposed methodology. Further validation included a comparison of the WMH volume difference between the total WMH volume and regional WMHs (summation of progression and regression). The difference between cross-sectional WMH volumes derived individually from the baseline and one-year images, demonstrated a strong relationship with the measurement of absolute WMH volume change ($r^2 = 0.988$, p-value < 0.001) further supporting the validity of the current methodology.

Finally, we assessed WMH progression, regression, and total WMH volume change in relation to longitudinal change in Trail Making Test A and B time to completion. These preliminary data showed that *both* greater progression and regression are potentially related

to declining Trail Making Test B performance over time. Although these results only trended toward significance in the small sample used for individual tests, the combined model including education and both growth and regression volumes explained about 13.5% of the variation in TMT-B difference scores in this sample. While a sex difference was found using backwards selection on the model with TMT A as the dependent variable, neither growth or regression WMH volumes were found to influence TMT A performance in this model. As such, the finding of sex differences in TMT A performance in this study appear to be an incidental finding of uncertain significance. Sex did not appear to have any influence on the methods for isolating WMH growth or regression volumes, nor were sex differences found to be important in the clinical validation of WMH growth and regression changes that influenced TMT B performance. Deficits on TMT-B, and other tests of executive function, are a prominent clinical feature of SVID (Lamar et al. 2010) and deficits in TMT-B performance in particular have been shown to be associated with WMH volumes (Ciulli et al. 2016, Duering et al. 2014). The present finding is intriguing in that it highlights the dynamic nature of WMHs when measured discretely by voxel as opposed to using aggregate WMH volume change scores. This result also sheds light on the importance of studying the longitudinal correlates of the WMH changes in relation to cognitive domain change over time and its potential contributions to the development of protocols designed to evaluate interventions that may influence WMH change, either through reducing WMH progression or in promoting WMH regression.

5. Conclusions:

The registration method developed here may ultimately aid our understanding of dynamic longitudinal volume and regional pattern WMH changes in older adults with varying degrees of CVD risks. Future work toward this goal will be required to develop statistical approaches to within-subject penumbra estimates that go beyond the simple voxel-level subtractions used here. Limitations of the present study include issues inherent in WMH post-processing techniques limiting analysis to individuals with scans devoid of significant brain atrophy, motion artifact, and extreme intensity variability between scans that may not be fully overcome using the present protocol. Further limitations include the lack of a broadly representative population that might inform on the generalizability of the findings in persons with disparate racial, ethnic and or socioeconomic status. Strengths include a rigorous approach focused on addressing the confounds of longitudinal volume and regional pattern analysis of WMH dynamic change, and broad distribution of subjects with heterogenous CVD risk factors required to effectively study dynamic WMH change over time.

Despite the limitations of the present study, the methods developed will help to advance the study of discrete, lesional, CVD-mediated, WMH change that has risen to critical importance in assessing the mixed contributions of degenerative and vascular disease states. Such mixed states are the norm rather than the exception in the vast majority of community-based cohorts at risk for cognitive decline and dementia (Abner et al. 2017, Schneider et al. 2009, Schneider et al. 2007). Future studies, afforded through the use of this protocol, will more fully explore the clinical utility of this protocol in identifying regional neuroanatomic WMH changes in relation to specific cerebrovascular risks, therapeutic interventions, and discrete clinical outcome measures that extend beyond TMT B.

Acknowledgments

This study was funded by NIH P30 AG028383, UH2 NS100606, and R01 AG042419

Abbreviations:

WMH	white matter hyperintensities
SVID	small vessel ischemic disease
CVD	cerebrovascular disease
FSL-BET	functional MRI software library-brain extraction tool
MRI	magnetic resonance imaging
TE	echo time
TI	inversion time
TR	repetition time
FLAIR	T2-weighted fluid-attenuated inversion recovery
MPRAGE	T1-weighted magnetization-prepared rapid acquisition gradient echo
SD	standard deviation
GM	gray matter
WM	white matter
CSF	cerebral spinal fluid
TMT	trail making test
TIV	total intercranial volume
ARIA	amyloid-related imaging abnormalities
ASL	arterial spin labelling
DTI	diffuse tensor imaging
BL	baseline
Y1	one-year

References

Abner EL, Kryscio RJ, Schmitt FA, Fardo DW, Moga DC, Ighodaro ET, Jicha GA, Yu L, Dodge HH, Xiong C, Woltjer RL, Schneider JA, Cairns NJ, Bennett DA, and Nelson PT. 2017. “Outcomes after diagnosis of mild cognitive impairment in a large autopsy series.” Ann Neurol 81 (4):549–559. doi: 10.1002/ana.24903. [PubMed: 28224671]

Al-Janabi OM, Bauer CE, Goldstein LB, Murphy RR, Bahrani AA, Smith CD, Wilcock DM, Gold BT, and Jicha GA. 2019. “White Matter Hyperintensity Regression: Comparison of Brain

Atrophy and Cognitive Profiles with Progression and Stable Groups." Brain Sci 9 (7). doi: 10.3390/brainsci9070170.

Ashburner J, and Friston KJ. 2005. "Unified segmentation." Neuroimage 26 (3):839–51. doi: 10.1016/j.neuroimage.2005.02.018. [PubMed: 15955494]

Ashburner J, and Ridgway GR. 2012. "Symmetric diffeomorphic modeling of longitudinal structural MRI." Front Neurosci 6:197. doi: 10.3389/fnins.2012.00197. [PubMed: 23386806]

Association, American Psychiatric. 2013. Diagnostic and statistical manual of mental disorders (DSM-5®). Vol. 5. Arlington, VA: American Psychiatric Association.

Bahrani AA, Al-Janabi OM, Abner EL, Bardach SH, Kryscio RJ, Wilcock DM, Smith CD, and Jicha GA. 2019. "Post-acquisition processing confounds in brain volumetric quantification of white matter hyperintensities." J Neurosci Methods 327:108391. doi: 10.1016/j.jneumeth.2019.108391. [PubMed: 31408649]

Bahrani AA, Powell DK, Yu G, Johnson ES, Jicha GA, and Smith CD. 2017. "White Matter Hyperintensity Associations with Cerebral Blood Flow in Elderly Subjects Stratified by Cerebrovascular Risk." J Stroke Cerebrovasc Dis 26 (4):779–786. doi: 10.1016/j.jstrokecerebrovasdis.2016.10.017. [PubMed: 28063772]

Baldaranov D, Khomenko A, Kobor I, Bogdahn U, Gorges M, Kassubek J, and Muller HP. 2017. "Longitudinal Diffusion Tensor Imaging-Based Assessment of Tract Alterations: An Application to Amyotrophic Lateral Sclerosis." Front Hum Neurosci 11:567. doi: 10.3389/fnhum.2017.00567. [PubMed: 29259550]

Beason-Held LL, Moghekar A, Zonderman AB, Kraut MA, and Resnick SM. 2007. "Longitudinal changes in cerebral blood flow in the older hypertensive brain." Stroke 38 (6):1766–73. doi: 10.1161/STROKEAHA.106.477109. [PubMed: 17510458]

Beg MF, and Khan A. 2007. "Symmetric data attachment terms for large deformation image registration." IEEE Trans Med Imaging 26 (9):1179–89. doi: 10.1109/TMI.2007.898813. [PubMed: 17896591]

Boyes RG, Gunter JL, Frost C, Janke AL, Yeatman T, Hill DL, Bernstein MA, Thompson PM, Weiner MW, Schuff N, Alexander GE, Killiany RJ, DeCarli C, Jack CR, Fox NC, and Adni Study. 2008. "Intensity non-uniformity correction using N3 on 3-T scanners with multichannel phased array coils." Neuroimage 39 (4):1752–62. doi: 10.1016/j.neuroimage.2007.10.026. [PubMed: 18063391]

Brickman AM, Muraskin J, and Zimmerman ME. 2009. "Structural neuroimaging in Altheimer's disease: do white matter hyperintensities matter?" Dialogues Clin Neurosci 11 (2):181–90. [PubMed: 19585953]

Brugulat-Serrat A, Salvado G, Operto G, Cacciaglia R, Sudre CH, Grau-Rivera O, Suarez-Calvet M, Falcon C, Sanchez-Benavides G, Gramunt N, Minguillon C, Fauria K, Barkhof F, Molinuevo JL, Gispert JD, and Alfa Study. 2020. "White matter hyperintensities mediate gray matter volume and processing speed relationship in cognitively unimpaired participants." Hum Brain Mapp 41 (5):1309–1322. doi: 10.1002/hbm.24877. [PubMed: 31778002]

Chen SP, Chou KH, Fuh JL, Huang YH, Huang CC, Lirng JF, Wang YF, Lin CP, and Wang SJ. 2018. "Dynamic Changes in White Matter Hyperintensities in Reversible Cerebral Vasoconstriction Syndrome." JAMA Neurol 75 (9):1106–1113. doi: 10.1001/jamaneurol.2018.1321. [PubMed: 29868878]

Ciulli S, Citi L, Salvadori E, Valenti R, Poggesi A, Inzitari D, Mascalchi M, Toschi N, Pantoni L, and Diciotti S. 2016. "Prediction of Impaired Performance in Trail Making Test in MCI Patients With Small Vessel Disease Using DTI Data." IEEE J Biomed Health Inform 20 (4):1026–33. doi: 10.1109/JBHI.2016.2537808. [PubMed: 26960231]

d'Arbeloff T, Elliott ML, Knodt AR, Melzer TR, Keenan R, Ireland D, Ramrakha S, Poulton R, Anderson T, Caspi A, Moffitt TE, and Hariri AR. 2019. "White matter hyperintensities are common in midlife and already associated with cognitive decline." Brain Commun 1 (1):fcz041. doi: 10.1093/braincomms/fcz041. [PubMed: 31894208]

Dickie DA, Ritchie SJ, Cox SR, Sakka E, Royle NA, Aribisala BS, Valdes Hernandez Mdel C, Maniega SM, Pattie A, Corley J, Starr JM, Bastin ME, Deary IJ, and Wardlaw JM. 2016. "Vascular risk factors and progression of white matter hyperintensities in the Lothian Birth Cohort 1936." Neurobiol Aging 42:116–23. doi: 10.1016/j.neurobiolaging.2016.03.011. [PubMed: 27143428]

Duering M, Gesierich B, Seiler S, Pirpamer L, Gonik M, Hofer E, Jouvent E, Duchesnay E, Chabriat H, Ropele S, Schmidt R, and Dichgans M. 2014. “Strategic white matter tracts for processing speed deficits in age-related small vessel disease.” Neurology 82 (22):1946–50. doi: 10.1212/WNL.0000000000000475. [PubMed: 24793184]

Gordon BA, Najmi S, Hsu P, Roe CM, Morris JC, and Benzinger TL. 2015. “The effects of white matter hyperintensities and amyloid deposition on Alzheimer dementia.” Neuroimage Clin 8:246–52. doi: 10.1016/j.nicl.2015.04.017. [PubMed: 26106548]

Greenberg DA 2014. “Cerebral angiogenesis: a realistic therapy for ischemic disease?” Methods Mol Biol 1135:21–4. doi: 10.1007/978-1-4939-0320-7_2. [PubMed: 24510851]

Gunstad J, Cohen RA, Tate DF, Paul RH, Poppas A, Hoth K, Macgregor KL, and Jefferson AL. 2005. “Blood pressure variability and white matter hyperintensities in older adults with cardiovascular disease.” Blood Press 14 (6):353–8. doi: 10.1080/08037050500364117. [PubMed: 16403689]

Habes M, Erus G, Toledo JB, Zhang T, Bryan N, Launer LJ, Rosseel Y, Janowitz D, Doshi J, Van der Auwera S, von Sarnowski B, Hegenscheid K, Hosten N, Homuth G, Volzke H, Schminke U, Hoffmann W, Grabe HJ, and Davatzikos C. 2016. “White matter hyperintensities and imaging patterns of brain ageing in the general population.” Brain 139 (Pt 4):1164–79. doi: 10.1093/brain/aww008. [PubMed: 26912649]

Hadj-Hamou M, Lorenzi M, Ayache N, and Pennec X. 2016. “Longitudinal Analysis of Image Time Series with Diffeomorphic Deformations: A Computational Framework Based on Stationary Velocity Fields.” Front Neurosci 10:236. doi: 10.3389/fnins.2016.00236. [PubMed: 27375408]

He JR, Zhang Y, Lu WJ, Liang HB, Tu XQ, Ma FY, Yang GY, and Zeng LL. 2017. “Age-Related Frontal Periventricular White Matter Hyperintensities and miR-92a-3p Are Associated with Early-Onset Post-Stroke Depression.” Front Aging Neurosci 9:328. doi: 10.3389/fnagi.2017.00328. [PubMed: 29051732]

Hutton C, Bork A, Josephs O, Deichmann R, Ashburner J, and Turner R. 2002. “Image distortion correction in fMRI: A quantitative evaluation.” Neuroimage 16 (1):217–40. doi: 10.1006/nimg.2001.1054. [PubMed: 11969330]

Iorio M, Spalletta G, Chiapponi C, Luccichenti G, Cacciari C, Orfei MD, Caltagirone C, and Piras F. 2013. “White matter hyperintensities segmentation: a new semi-automated method.” Front Aging Neurosci 5:76. doi: 10.3389/fnagi.2013.00076. [PubMed: 24339815]

Kalaria RN, and Erkinjuntti T. 2006. “Small vessel disease and subcortical vascular dementia.” J Clin Neurol 2 (1):1–11. doi: 10.3988/jcn.2006.2.1.1. [PubMed: 20396480]

Kandel BM, Avants BB, Gee JC, McMillan CT, Erus G, Doshi J, Davatzikos C, and Wolk DA. 2016. “White matter hyperintensities are more highly associated with preclinical Alzheimer’s disease than imaging and cognitive markers of neurodegeneration.” Alzheimers Dement (Amst) 4:18–27. doi: 10.1016/j.dadm.2016.03.001. [PubMed: 27489875]

Keihaninejad S, Zhang H, Ryan NS, Malone IB, Modat M, Cardoso MJ, Cash DM, Fox NC, and Ourselin S. 2013. “An unbiased longitudinal analysis framework for tracking white matter changes using diffusion tensor imaging with application to Alzheimer’s disease.” Neuroimage 72:153–63. doi: 10.1016/j.neuroimage.2013.01.044. [PubMed: 23370057]

Kirshner HS, and Bradshaw M. 2015. “The Inflammatory Form of Cerebral Amyloid Angiopathy or “Cerebral Amyloid Angiopathy-Related Inflammation” (CAARI).” Curr Neurol Neurosci Rep 15 (8):54. doi: 10.1007/s11910-015-0572-y. [PubMed: 26096511]

Lamar M, Price CC, Giovannetti T, Swenson R, and Libon DJ. 2010. “The dysexecutive syndrome associated with ischaemic vascular disease and related subcortical neuropathology: a Boston process approach.” Behav Neurol 22 (1–2):53–62. doi: 10.3233/BEN-2009-0237. [PubMed: 20543459]

Lauer A, Speroni SL, Patel JB, Regalado E, Choi M, Smith E, Kalpathy-Kramer J, Caruso P, Milewicz DM, and Musolino PL. 2021. “Cerebrovascular Disease Progression in Patients With ACTA2 Arg179 Pathogenic Variants.” Neurology 96 (4):e538–e552. doi: 10.1212/WNL.0000000000011210. [PubMed: 33199432]

Lee S, Zimmerman ME, Narkhede A, Nasrabady SE, Tosto G, Meier IB, Benzinger TLS, Marcus DS, Fagan AM, Fox NC, Cairns NJ, Holtzman DM, Buckles V, Ghetti B, McDade E, Martins RN, Saykin AJ, Masters CL, Ringman JM, Frster S, Schofield PR, Sperling RA, Johnson KA, Chhatwal JP, Salloway S, Correia S, Jack CR Jr., Weiner M, Bateman RJ, Morris JC,

Mayeux R, Brickman AM, and Network Dominantly Inherited Alzheimer. 2018. “White matter hyperintensities and the mediating role of cerebral amyloid angiopathy in dominantly-inherited Alzheimer’s disease.” PLoS One 13 (5):e0195838. doi: 10.1371/journal.pone.0195838. [PubMed: 29742105]

Maillard P, Carmichael O, Fletcher E, Reed B, Mungas D, and DeCarli C. 2012. “Coevolution of white matter hyperintensities and cognition in the elderly.” Neurology 79 (5):442–8. doi: 10.1212/WNL.0b013e3182617136. [PubMed: 22815562]

Maillard P, Carmichael O, Harvey D, Fletcher E, Reed B, Mungas D, and DeCarli C. 2013. “FLAIR and diffusion MRI signals are independent predictors of white matter hyperintensities.” AJNR Am J Neuroradiol 34 (1):54–61. doi: 10.3174/ajnr.A3146. [PubMed: 22700749]

Maillard P, Fletcher E, Harvey D, Carmichael O, Reed B, Mungas D, and DeCarli C. 2011. “White matter hyperintensity penumbra.” Stroke 42 (7):1917–22. doi: 10.1161/STROKEAHA.110.609768. [PubMed: 21636811]

Makarewicz KA, Zaryczanska K, Machowska-Sempruch K, Bajer-Czajkowska A, Golofit P, Gabrysz-Trybek E, and Nowacki P. 2019. “Cerebral amyloid angiopathy-related inflammation (CAARI): case report.” Folia Neuropathol 57 (2):205–210. doi: 10.5114/fn.2019.86297. [PubMed: 31556579]

Maltbie E, Bhatt K, Paniagua B, Smith RG, Graves MM, Mosconi MW, Peterson S, White S, Blocher J, El-Sayed M, Hazlett HC, and Styner MA. 2012. “Asymmetric bias in user guided segmentations of brain structures.” Neuroimage 59 (2):1315–23. doi: 10.1016/j.neuroimage.2011.08.025. [PubMed: 21889995]

Mills KL, and Tamnes CK. 2014. “Methods and considerations for longitudinal structural brain imaging analysis across development.” Dev Cogn Neurosci 9:172–90. doi: 10.1016/j.dcn.2014.04.004. [PubMed: 24879112]

Moroni F, Ammirati E, Rocca MA, Filippi M, Magnoni M, and Camici PG. 2018. “Cardiovascular disease and brain health: Focus on white matter hyperintensities.” Int J Cardiol Heart Vasc 19:63–69. doi: 10.1016/j.ijcha.2018.04.006. [PubMed: 29946567]

Murray ME, Vemuri P, Preboske GM, Murphy MC, Schweitzer KJ, Parisi JE, Jack CR Jr., and Dickson DW. 2012. “A quantitative postmortem MRI design sensitive to white matter hyperintensity differences and their relationship with underlying pathology.” J Neuropathol Exp Neurol 71 (12):1113–22. doi: 10.1097/NEN.0b013e318277387e. [PubMed: 23147507]

Nasrabady SE, Rizvi B, Goldman JE, and Brickman AM. 2018. “White matter changes in Alzheimer’s disease: a focus on myelin and oligodendrocytes.” Acta Neuropathol Commun 6 (1):22. doi: 10.1186/s40478-018-0515-3. [PubMed: 29499767]

Pandit L 2009. “Differential diagnosis of white matter diseases in the tropics: An overview.” Ann Indian Acad Neurol 12 (1):12–21. doi: 10.4103/0972-2327.48846. [PubMed: 20151003]

Prabhakaran S 2019. “Blood Pressure, Brain Volume and White Matter Hyperintensities, and Dementia Risk.” JAMA 322 (6):512–513. doi: 10.1001/jama.2019.10849. [PubMed: 31408120]

Raman MR, Himali JJ, Conner SC, DeCarli C, Vasan RS, Beiser AS, Seshadri S, Maillard P, and Satizabal CL. 2018. “Circulating Vascular Growth Factors and Magnetic Resonance Imaging Markers of Small Vessel Disease and Atrophy in Middle-Aged Adults.” Stroke 49 (9):2227–2229. doi: 10.1161/STROKEAHA.118.022613. [PubMed: 30354979]

Ramirez J, McNeely AA, Berezuk C, Gao F, and Black SE. 2016. “Dynamic Progression of White Matter Hyperintensities in Alzheimer’s Disease and Normal Aging: Results from the Sunnybrook Dementia Study.” Front Aging Neurosci 8:62. doi: 10.3389/fnagi.2016.00062. [PubMed: 27047377]

Rigney L, Sebire D, and Cordato D. 2015. “Acute dysphasia and reversible cognitive decline in a patient with probable cerebral amyloid angiopathy-related inflammation. Case Rep Neurol Med 2015:189581. doi: 10.1155/2015/189581. [PubMed: 25821615]

Rost NS, Sadaghiani S, Biffi A, Fitzpatrick KM, Cloonan L, Rosand J, Shibata DK, and Mosley TH Jr. 2014. “Setting a gold standard for quantification of leukoaraiosis burden in patients with ischemic stroke: the Atherosclerosis Risk in Communities Study.” J Neurosci Methods 221:196–201. doi: 10.1016/j.jneumeth.2013.10.009. [PubMed: 24459720]

Sarbu N, Shih RY, Jones RV, Horkayne-Szakaly I, Oleaga L, and Smirniotopoulos JG. 2016. “White Matter Diseases with Radiologic-Pathologic Correlation.” Radiographics 36 (5):1426–47. doi: 10.1148/rg.2016160031. [PubMed: 27618323]

Saver JL 2017. “Penumbral salvage and thrombolysis outcome: a drop of brain, a week of life.” Brain 140 (3):519–522. doi: 10.1093/brain/awx020. [PubMed: 28364555]

Schmitt FA, Nelson PT, Abner E, Scheff S, Jicha GA, Smith C, Cooper G, Mendiondo M, Danner DD, Van Eldik LJ, Caban-Holt A, Lovell MA, and Kryscio RJ. 2012. “University of Kentucky Sanders-Brown healthy brain aging volunteers: donor characteristics, procedures and neuropathology.” Curr Alzheimer Res 9 (6):724–33. doi: 10.2174/156720512801322591. [PubMed: 22471862]

Schneider JA, Aggarwal NT, Barnes L, Boyle P, and Bennett DA. 2009. “The neuropathology of older persons with and without dementia from community versus clinic cohorts.” J Alzheimers Dis 18 (3):691–701. doi: 10.3233/JAD-2009-1227. [PubMed: 19749406]

Schneider JA, Arvanitakis Z, Bang W, and Bennett DA. 2007. “Mixed brain pathologies account for most dementia cases in community-dwelling older persons.” Neurology 69 (24):2197–204. doi: 10.1212/01.wnl.0000271090.28148.24. [PubMed: 17568013]

Silbert LC, Nelson C, Howieson DB, Moore MM, and Kaye JA. 2008. “Impact of white matter hyperintensity volume progression on rate of cognitive and motor decline.” Neurology 71 (2):108–13. doi: 10.1212/01.wnl.0000316799.86917.37. [PubMed: 18606964]

Sled JG, Zijdenbos AP, and Evans AC. 1998. “A nonparametric method for automatic correction of intensity nonuniformity in MRI data.” IEEE Trans Med Imaging 17 (1):87–97. doi: 10.1109/42.668698. [PubMed: 9617910]

Smith CD, Johnson ES, Van Eldik LJ, Jicha GA, Schmitt FA, Nelson PT, Kryscio RJ, Murphy RR, and Wellnitz CV. 2016. “Peripheral (deep) but not periventricular MRI white matter hyperintensities are increased in clinical vascular dementia compared to Alzheimer’s disease.” Brain Behav 6 (3):e00438. doi: 10.1002/brb3.438. [PubMed: 26925303]

R: A language and environment for statistical computing 4.0.0. R Foundation for Statistical Computing, Vienna, Austria.

Trip SA, and Miller DH. 2005. “Imaging in multiple sclerosis.” J Neurol Neurosurg Psychiatry 76 Suppl 3:iii11–iii18. doi: 10.1136/jnnp.2005.073213. [PubMed: 16107385]

Tsai JZ, Peng SJ, Chen YW, Wang KW, Li CH, Wang JY, Chen CJ, Lin HJ, Smith EE, Wu HK, Sung SF, Yeh PS, and Hsin YL. 2014. “Automated segmentation and quantification of white matter hyperintensities in acute ischemic stroke patients with cerebral infarction.” PLoS One 9 (8):e104011. doi: 10.1371/journal.pone.0104011. [PubMed: 25127120]

Tsai YH, Yuan R, Huang YC, Weng HH, Yeh MY, Lin CP, and Biswal BB. 2014. “Altered resting-state FMRI signals in acute stroke patients with ischemic penumbra.” PLoS One 9 (8):e105117. doi: 10.1371/journal.pone.0105117. [PubMed: 25121486]

Valdes Hernandez MDC, Chappell FM, Munoz Maniega S, Dickie DA, Royle NA, Morris Z, Anblagan D, Sakka E, Armitage PA, Bastin ME, Deary IJ, and Wardlaw JM. 2017. “Metric to quantify white matter damage on brain magnetic resonance images.” Neuroradiology 59 (10):951–962. doi: 10.1007/s00234-017-1892-1. [PubMed: 28815362]

van Leijsen EM, Bergkamp MI, van Uden IW, Cooijmans S, Ghafoorian M, van der Holst HM, Norris DG, Kessels RP, Platel B, Tuladhar AM, and de Leeuw FE. 2019. “Cognitive consequences of regression of cerebral small vessel disease.” Eur Stroke J 4 (1):85–89. doi: 10.1177/2396987318820790. [PubMed: 31165098]

van Leijsen EMC, van Uden IWM, Ghafoorian M, Bergkamp MI, Lohner V, Kooijmans ECM, van der Holst HM, Tuladhar AM, Norris DG, van Dijk EJ, Rutten-Jacobs LCA, Platel B, Klijn CJM, and de Leeuw FE. 2017. “Nonlinear temporal dynamics of cerebral small vessel disease: The RUN DMC study.” Neurology 89 (15):1569–1577. doi: 10.1212/WNL.0000000000004490. [PubMed: 28878046]

Wang Y, Yang Y, Wang T, Nie S, Yin H, and Liu J. 2020. “Correlation between White Matter Hyperintensities Related Gray Matter Volume and Cognition in Cerebral Small Vessel Disease.” J Stroke Cerebrovasc Dis 29 (12):105275. doi: 10.1016/j.jstrokecerebrovasdis.2020.105275. [PubMed: 32992182]

Wardlaw JM, Chappell FM, Valdes Hernandez MDC, Makin SDJ, Staals J, Shuler K, Thrippleton MJ, Armitage PA, Munoz-Maniega S, Heye AK, Sakka E, and Dennis MS. 2017. "White matter hyperintensity reduction and outcomes after minor stroke." Neurology 89 (10):1003–1010. doi: 10.1212/WNL.0000000000004328. [PubMed: 28794252]

Wardlaw JM, Valdes Hernandez MC, and Munoz-Maniega S. 2015. "What are white matter hyperintensities made of? Relevance to vascular cognitive impairment." J Am Heart Assoc 4 (6):001140. doi: 10.1161/JAHA.114.001140. [PubMed: 26104658]

Wickham H 2016. ggplot2: elegant graphics for data analysis. 2 vols. Vol. 2: springer.

Williamson W, Lewandowski AJ, Forkert ND, Griffanti L, Okell TW, Betts J, Boardman H, Siepmann T, McKean D, Huckstep O, Francis JM, Neubauer S, Phellan R, Jenkinson M, Doherty A, Dawes H, Frangou E, Malamateniou C, Foster C, and Leeson P. 2018. "Association of Cardiovascular Risk Factors With MRI Indices of Cerebrovascular Structure and Function and White Matter Hyperintensities in Young Adults." JAMA 320 (7):665–673. doi: 10.1001/jama.2018.11498. [PubMed: 30140877]

Winblad B, Palmer K, Kivipelto M, Jelic V, Fratiglioni L, Wahlund LO, Nordberg A, Backman L, Albert M, Almkvist O, Arai H, Basun H, Blennow K, de Leon M, DeCarli C, Erkinjuntti T, Giacobini E, Graff C, Hardy J, Jack C, Jorm A, Ritchie K, van Duijn C, Visser P, and Petersen RC. 2004. "Mild cognitive impairment--beyond controversies, towards a consensus: report of the International Working Group on Mild Cognitive Impairment." J Intern Med 256 (3):240–6. doi: 10.1111/j.1365-2796.2004.01380.x. [PubMed: 15324367]

Wintermark M, Flanders AE, Velthuis B, Meuli R, van Leeuwen M, Goldsher D, Pineda C, Serena J, van der Schaaf I, Waaijer A, Anderson J, Nesbit G, Gabriely I, Medina V, Quiles A, Pohlman S, Quist M, Schnyder P, Bogousslavsky J, Dillon WP, and Pedraza S. 2006. "Perfusion-CT assessment of infarct core and penumbra: receiver operating characteristic curve analysis in 130 patients suspected of acute hemispheric stroke." Stroke 37 (4):979–85. doi: 10.1161/01.STR.0000209238.61459.39. [PubMed: 16514093]

Zhao Y, Ke Z, He W, and Cai Z. 2019. "Volume of white matter hyperintensities increases with blood pressure in patients with hypertension." J Int Med Res 47 (8):3681–3689. doi: 10.1177/0300060519858023. [PubMed: 31242795]

Zhong Y, Utriainen D, Wang Y, Kang Y, and Haacke EM. 2014. "Automated White Matter Hyperintensity Detection in Multiple Sclerosis Using 3D T2 FLAIR." Int J Biomed Imaging 2014:239123. doi: 10.1155/2014/239123. [PubMed: 25136355]

HIGHLIGHTS

- Midpoint co-registration of FLAIR images can be used to assess longitudinal WMH changes
- Image intensity z-score corrections minimize co-registration T2 signal artifacts
- Dynamic intra-subject WMH volume changes include a mix of both progression and regression
- WMH progression is associated with a decline in executive function
- This standardized protocol can accurately detect such changes over a short one-year interval

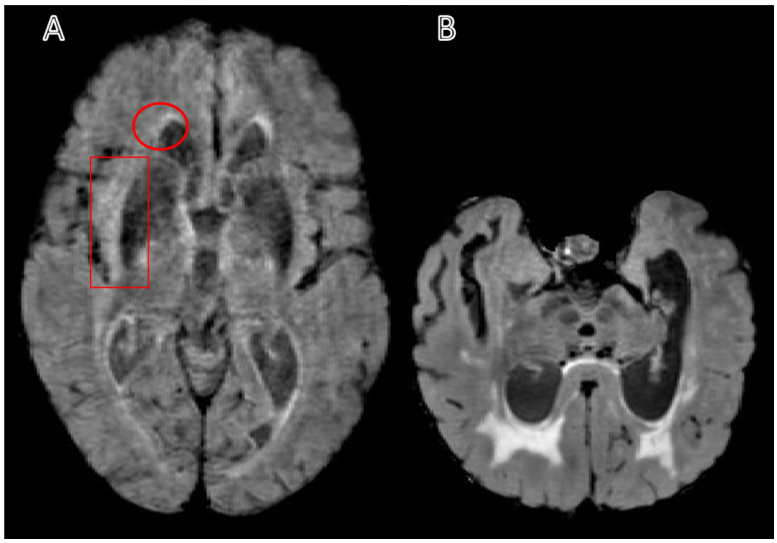

Fig. 1:

Sample of the excluded T2-weighted fluid-attenuated inversion recovery (FLAIR) images. A) A FLAIR image with a motion artifact leads to undefined ventricles and white matter hyperintensities edges (see the circle). Also, the motion artifact could lead to a variation in the intensity that may appear as a WMH and may cause an overestimation volume (see the rectangle). (B) A FLAIR image shows an irregular brain shape and ventricles that can cause a segmentation error.

Note: The motion artifact in panel A can be compared to panel B, and the asymmetry in panel B can be compared to panel A.

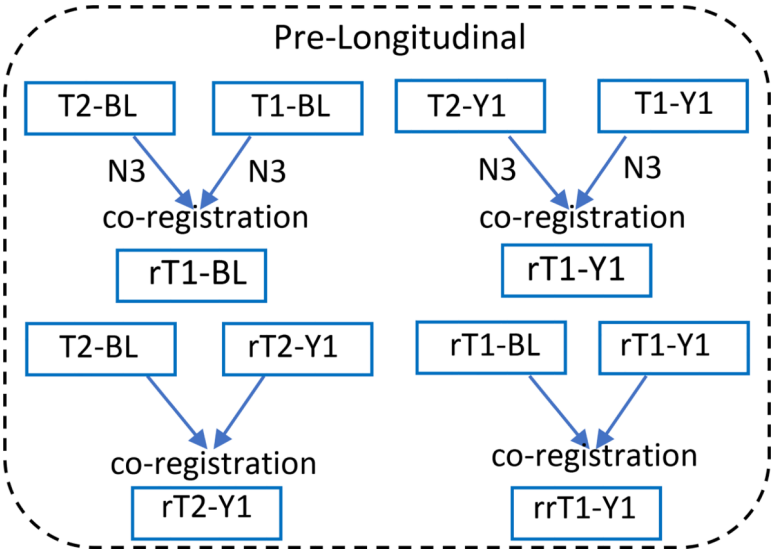

Fig. 2:

Pre-longitudinal registration step. T2-BL, -Y1 (T2-weighted image, FLAIR, baseline, year one visit). T1-BL, -Y1 (T1-weighted, MPRAGE image, baseline, year one visit). This step divided into two parts: First, intensity correction (N3) for all the images and co-registering the T1 and T2 for each time point separately. Second, registering each one-year visit imaging sequence (T1 or T2) to the baseline.

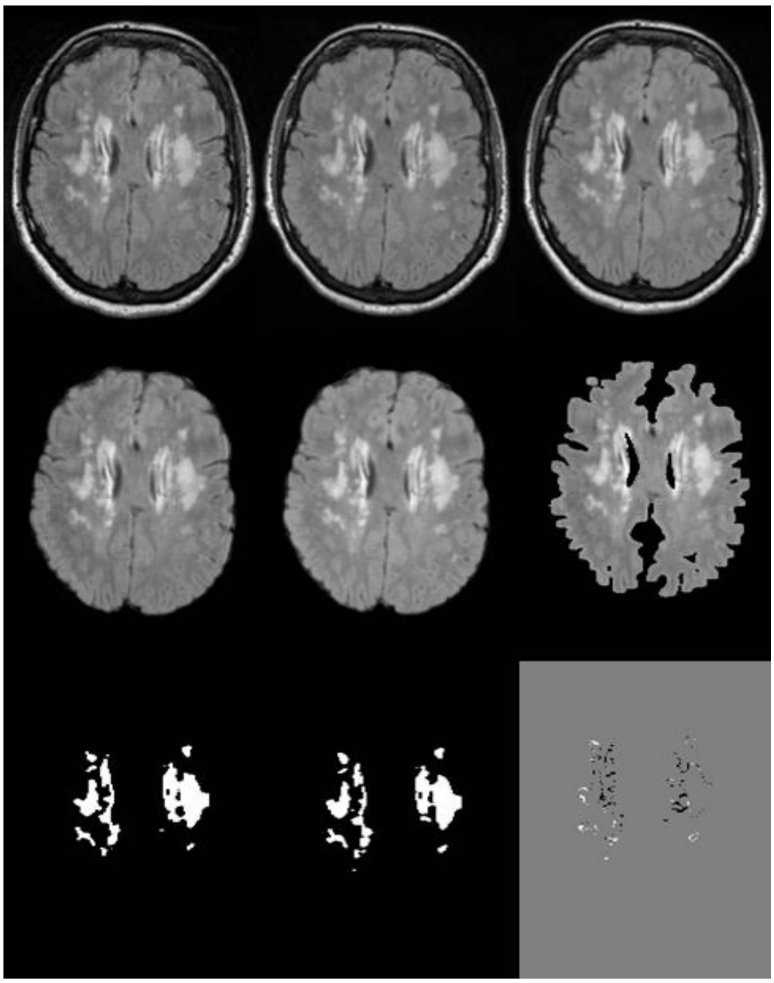

Fig. 3:

The main output steps of the penumbra protocol. A and B are the FLAIR images of the twotime-points before the longitudinal step. C is the midpoint image of the two FLAIR images of the longitudinal step. D and E are the longitudinal registered images of the two-time-points after stripping the nonbrain tissue. F is the white matter mask after segmentation step (normal appearing WM and WMH). G and H are the WMH masks of the two-time-points. I is the regional pattern penumbra (white) and regression (black) masks after subtracting WMH masks at time-2 and time-1 from each other.

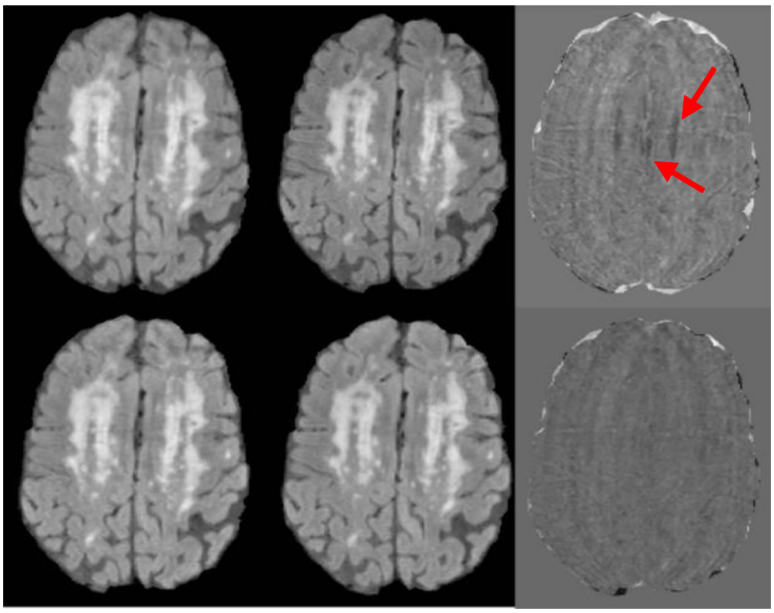

Fig. 4:

The z-score of the FLAIR images from baseline and year 1 scans. A and B are the normalized FLAIR images of a two-time-points before longitudinal registration. C is the z-score difference of the two-time-points before registration. D and E are the normalized FLAIR images of a two-time-points after longitudinal registration and F is z-score difference image. Red arrows show the result of subtraction of the two normalized images before longitudinal registration due to the poor alignment.

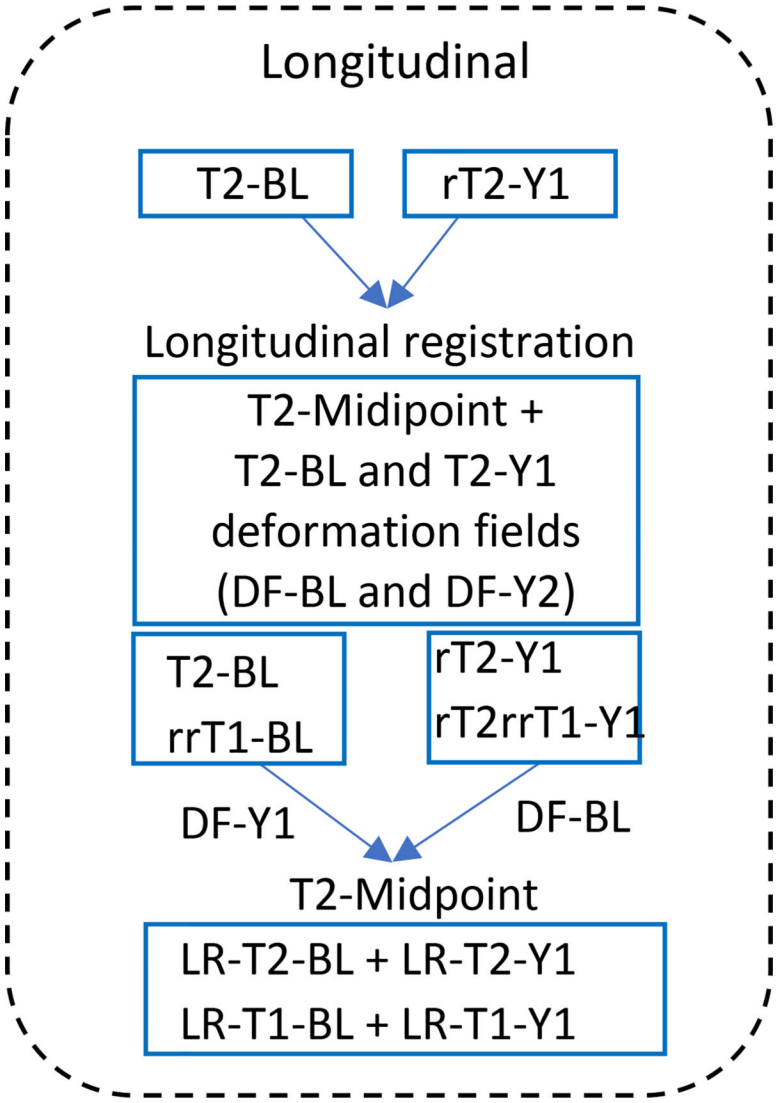

Fig. 5:

Longitudinal registration step. T2-BL, -Y1 (T2-weighted image, FLAIR, baseline, one-yearvisit). T1-BL, -Y1 (T1-weighted image, baseline, one-year-visit). DF, deformation field. LR, longitudinal registration. The T2-weighted FLAIR images (T2-BL and rT2-Y1) from the preregistration step registered longitudinally to generate the midpoint image (T2-Midpoint) and the deformation field of each time point (DF-Y1 and DF-BL). Applying the deformation filed of each time point to register all images to the midpoint image, to get the longitudinal registered images (LR-T2-BL, LR-T1-BL, LR-T2-Y1, and LR-T2-Y1).

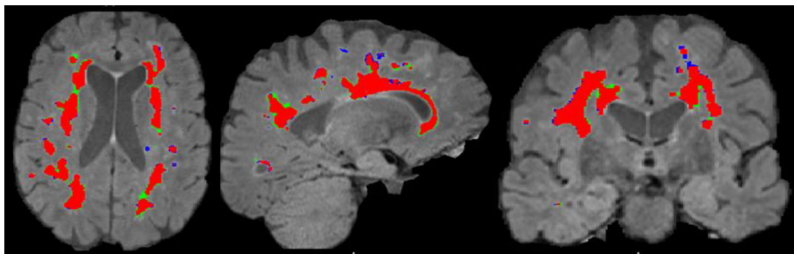

Fig. 6:

WMH masks from a single representative subject overlaid on their FLAIR image. Red: WMH static, Blue: WMH regression and, Green: WMH growth.

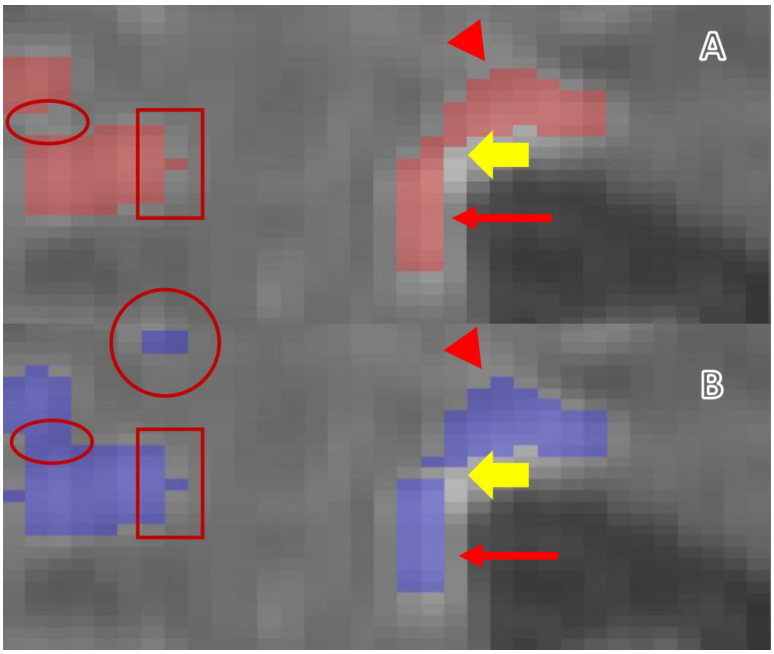

Fig. 7:

An example of year 1 WMH voxels overlaid on a baseline FLAIR image. A: Baseline. B: One-year. The narrow arrows show the edge of the WMH bordering the ventricles. A: Baseline. B: One-year. The narrow arrows show the edge of the WMH bordering the ventricles. The full yellow arrows indicate the regression of the WMH at one-year visit (changes inside the WMH cluster). The arrowheads show the changes of the WMH toward the deep WM. The rectangles show stable WMH. The circle shows the appearance of a new WMH (Penumbra). The ellipsoids show the penumbra inside the WMH cluster.

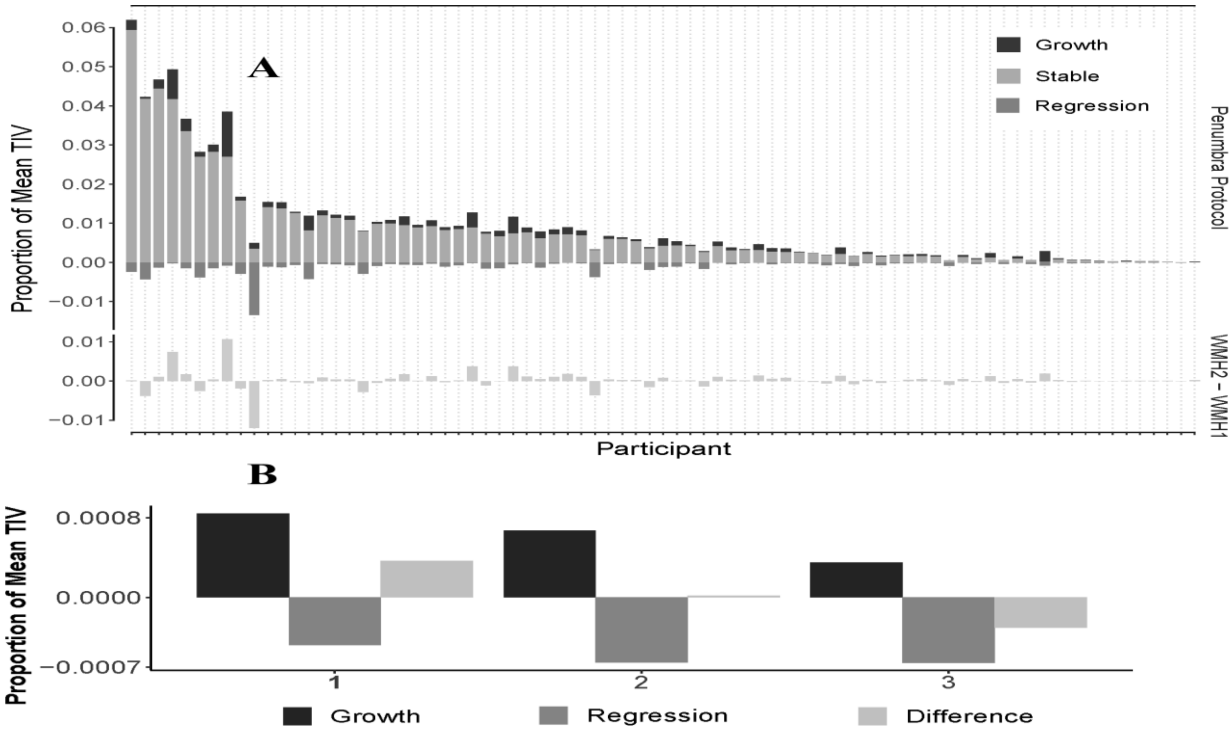

Fig. 8:

Longitudinal WMH for 79 participants. **A)** Participants are sorted greatest to least (left to right) by total WMH at first scan (i.e., WMH1 / TIV1). The top row of panels shows the growth, stable, and regression segmentations of WMH, as a proportion of mean TIV. The bottom row of panels shows the total WMH change as a proportion of mean TIV. **B)** Three different cases with WMH2-WMH1 compared to the longitudinal WMH results that demonstrate both growth and regression in WMH whereas the WMH difference shows only a single volume.

Table 1.

Basic demographic features at the time of the baseline scan for the participants analyzed in this study.

	All Participants (*n* = 79)
Age (mean years ± SD)	74.01 (7.6)
Education (mean years ± SD)	16.11 (2.8)
Female (n, %)	42 (53.1%)
Black (n, %)	3 (3.7%)
History of Hypertension (n, %)	57 (72.2%)
History of Hypercholesterolemia (n, %)	51 (64.6%)
History of Diabetes (n, %)	17 (21.5%)
History of Remote Stroke (n, %)	9 (11.4%)
MMSE (mean ± SD)	27.1 (3.4)
Total WMH as % of TIV (mean ± SD)	0.89 (1.18)
Cognitively Intact (n, %)	39 (49.3%)
Mild Cognitive Impairment (n, %)	36 (45.6%)
Dementia (n, %)	4 (5%)